
Article:
Taylor-Mew, J., Li, L., Blain, T. et al. (2025) Room temperature InGaAs/AlGaAsSb Single Photon Avalanche Diode. IEEE Photonics Journal, 17 (2). 2000106. ISSN: 1943-0647

https://doi.org/10.1109/jphot.2025.3541323

Room Temperature InGaAs/AlGaAsSb Single Photon Avalanche Diode

J. Taylor-Mew, L. Li, T. Blain, C. H. Tan, *Senior Member, IEEE*, and J. S. Ng, *Member, IEEE*

***Abstract*—Near-infrared Single Photon Avalanche Diodes (SPADs) are the dominant, practical single photon detectors for quantum applications and low-level optical sensing. Although some infrared SPADs can operate at room temperature, thermoelectric coolers are still essential, increasing complexity (operation and device packaging) and power consumption. Passively-cooled SPADs could be realized by avalanche materials exhibiting better temperature stability. A promising candidate is the InGaAs/AlGaAsSb SPAD, because the AlGaAsSb multiplier is highly stable with temperature. In this work, we report single photon detection performance of InGaAs/AlGaAsSb SPADs at room temperature and 1550 nm wavelength using multiple devices for each type of measurements. With 0.1 photons per pulse and 15 μm diameter devices, the maximum SPDE was 14% at DCR of 30 Mc.s^{-1}, respectively. The best NEP value is around an order of magnitude higher than InGaAs/InP SPADs, but are comparable to InGaAs/InAlAs SPADs. Within the relevant overbias range and repetition rate up to 1 MHz, the DCR was unaffected by afterpulsing. Timing jitters were as low as 150 ps, matching InGaAs/InP SPADs. The results of this work are much more competitive than the previous report of InGaAs/AlGaAsSb SPAD, which required cooling to 200 K to detect single photons. Further research could help InGaAs/AlGaAsSb SPADs progressing towards passively-cooled single photon detectors for room temperature operation.**

***Index Terms*—AlGaAsSb, Geiger mode avalanche photodiode, room temperature, single photon avalanche diode (SPAD), single photon detection efficiency (SPDE).**

I. Introduction

SINGLE photon detectors are crucial for applications relying on single photon counting (e.g., Quantum Key Distribution [1]) or detection of weak optical pulses down to few-photon-level (e.g., laser ranging [2], [3] and remote gas sensing [4]). Many applications operate at ∼1550 nm to utilize the low-loss window in optical fibers or minimize optical attenuation caused by atmospheric obscurants in free-space systems. At this wavelength, the best performance is offered by Superconducting Nanowire Single Photon Detectors (SNSPDs), with single photon detection efficiency (SPDE) ∼90 % and very low false or Dark Count Rate (DCR) when optical cavity and anti-reflecting coating were incorporated [5]. However, their cryogenic operation temperatures (< 4 K) severely limit their adoption.

The other dominant single photon counting detector technology, Single Photon Avalanche Diodes (SPADs), can operate at significantly higher temperatures, between 200 K and room temperature. Thus, inexpensive thermoelectric coolers are used to cool and maintain the SPAD temperature. Nevertheless, thermoelectric coolers degrade the power efficiency of the SPAD module and increase the complexity of device packaging. For single photon detection at 1550 nm wavelength, $In_{0.53}Ga_{0.47}As$/InP SPADs provide the best combinations of DCR-SPDE values [6], [7], [8], [9], [10], [11], [12], [13] and are available commercially.

Research efforts have improved the performance of $In_{0.53}Ga_{0.47}As$/InP SPADs such that some of them are now able to operate at Room Temperature (RT) with reasonable DCR values (500 - 760 kcps) and SPDE up to 60.4% at 1550 nm wavelength [6], [7], [8], [9], [10], [14], [15], [16]. Increasing the operation temperature to room temperature is highly desirable because it reduces the operation complexity and power consumption of the SPAD modules. Higher operation temperature can also improve SPAD performance significantly because the undesirable afterpulsing effect is much reduced at room temperature compared to lower temperatures [11], [12].

$In_{0.53}Ga_{0.47}As$/InP SPADs operating at room temperature still require thermal stabilizing components due to InP having relatively large temperature coefficients of breakdown voltage (∼100's mV.K^{-1}) [13]. Hence, it is desirable to explore SPADs made with alternative avalanche materials that have better temperature stability. Attempts to improve SPAD's temperature stability led to investigations into $In_{0.53}Ga_{0.47}As$/InAlAs SPADs (which offer lower temperature coefficients of breakdown voltage ∼20–50 mV.K^{-1} [17], [18]) and InAlAs-based SPADs operated at RT have been reported [17], [19], [20], [21].

Ge/Si SPADs can also operate at room temperature [22], [23], although much of the better performance values were at 1310 nm wavelength (e.g., peak SPDE of 25% with a DCR of 7.2 Mc.s^{-1} [22]). Recently, an $Al_{0.85}Ga_{0.15}As_{0.56}Sb_{0.44}$ (AlGaAsSb) avalanche photodiode originally designed for linear-mode operation [24] achieved single photon detection at 200 K when operated in Geiger-mode [25]. The avalanche material of AlGaAsSb is highly stable with temperature [25], [26], leading to AlGaAsSb APDs with stable avalanche gain and low noise even when operated at 85 °C [27]. Hence, an AlGaAsSb-based SPAD offers the potential of 1550 nm wavelength SPADs operating at room temperature, in turn enabling a thermoelectric cooler-free SPAD. In this work, we report data of

Received 24 January 2025; accepted 8 February 2025. Date of publication 13 February 2025; date of current version 27 February 2025. This work was supported by U.K. Research and Innovation under Project 10031973. *(Corresponding author: J. S. Ng.)*

The authors are with the School of Electrical and Electronic Engineering, The University of Sheffield, S1 3JD Sheffield, U.K. (e-mail: j.taylor-mew@sheffield.ac.uk; lli52@sheffield.ac.uk; t.blain@sheffield.ac.uk; c.h.tan@sheffield.ac.uk; j.s.ng@sheffield.ac.uk).

Digital Object Identifier 10.1109/JPHOT.2025.3541323

single photon detection from $In_{0.53}Ga_{0.47}As$/AlGaAsSb SPADs operated at 300 K, including DCR, SPDE, avalanche event timing distribution, and afterpulsing effect. The data reported in this manuscript is available from ORDA digital repository [27].

II. Experimental Details

The SPAD devices were acquired from Phlux Technology Ltd, which designed and fabricated the devices. We were informed that the wafer was grown on a semi-insulating InP substrate using molecular beam epitaxy. The wafer was fabricated into mesa devices with 15 to 55 μm diameters and all devices have anti-reflection coating designed for 1550 nm wavelength light. The devices use an InGaAs layer for photon absorption. A charge sheet separates the InGaAs absorption layer and the AlGaAsSb avalanche layer, minimizing the absorber's electric field and hence band-to-band tunneling current. The wafer of this work was designed to have lower electric field in the InGaAs absorption layer compared to the wafer in our previous work, which was designed to function as a linear mode APD [25].

All device characterization was carried out in a probe station with a sample stage heated to 300 K for all measurements unless otherwise stated. Linear mode characterization included dark current and multiplied responsivity, R, as functions of reverse bias V_b. The dark current measurements were carried out on multiple devices with diameters ranging from 15 to 55 μm, to determine device uniformity and approximate breakdown voltage, V_{br}. For the $R(V_b)$ measurements, a 1550 nm wavelength laser was the optical source, and avalanche current was measured using a phase-sensitive detection method (implemented with modulated laser light and lock-in amplifier). R-V_b data were obtained from 6 devices (with 55 μm diameter), and the data were subsequently used to ensure single photon injection conditions in SPDE measurements. In addition, a raster scan of photocurrent (using an optical spot of $\sim$5 μm) was performed on a 35 μm diameter device reverse-biased at 58.5 V (0.975V_{bd}, in linear mode) to check for the presence of electric field hot spots. Again, the optical source was a modulated 1550 nm wavelength laser and phase-sensitive detection was used to measure the photocurrent.

Geiger mode characterization at 300 K included DCR, SPDE, avalanche event's timing distribution, and afterpulsing effects as functions of overbias, V_{ov}. For DCR and SPDE, six devices with diameters of 15 and 35 μm (three devices for each diameter) were measured. These were carried out using the cryogenic probe station setup described in [17], with an additional optical fiber for ease of monitoring of optical power delivered to the device-under-test (DUT). The DUT was reverse-biased in gated mode via a bias-tee to superimpose gate voltage pulses, V_{ac}, onto a d.c. bias, V_{dc}. The gate pulses had a nominal on-time, t_{on}, of 20 ns (including rise time of 5 ns and fall time of 5 ns) with a repetition rate, f of 10 kHz. V_{ac} and V_{dc} were selected so that $V_{dc} < V_{br}$ and $(V_{ac} + V_{dc}) > V_{br}$. The effective V_{ov} applied to the DUT was given by $V_{ov} = (V_{ac}+V_{dc})$ - V_{br} and adjustments in V_{dc} yielded changes in V_{ov}. To exclude portions of the gate voltage pulses below V_{br}, t_{on} values were adjusted to 11–20 ns (based on experimental calibrations of the setup) in subsequent DCR calculations.

The avalanche currents from the DUT were detected as avalanche events (whether due to dark carriers or photons) by an edge-triggered discriminator. Capacitive transients (caused by the rising and falling edges of the gate pulses) present in the avalanche signals at the discriminator's input were reduced significantly, allowing smaller breakdown events to be detected and counted. The reduction was achieved by the generation of capacitive transients (through a variable capacitor, wide bandwidth voltage attenuators, and appropriate lengths of electrical cables), followed by a high-speed differential amplifier for transient cancellations (similar to the circuit design of [28]). When the DUT was in the dark, the gated measurements yielded the gated dark counts per second, C_{dark}. Using $\mathrm{DCR} = -[\ln(1 - C_{dark}/f)]/t_{on}$ [28], DCR estimated for free-running operation was obtained. Some Geiger-mode DCR measurements were carried out in free-running method, i.e., the DUT was reverse-biased by only a d.c bias. In the free-running measurements, the avalanche currents were quenched using a 360 kΩ series resistor and $\mathrm{DCR} = C_{dark}$.

All SPDE measurements were carried out in gated biasing method and used a 1566.5 nm pulsed laser (pulse width $\sim$23 ps). A combination of fixed and variable optical attenuators ensured the mean number of photons per pulse, $\bar{N}$, injected into the DUT was 0.1, minimizing the probability of injecting more than 1 photon within a pulse into the DUT (which would have invalidated the SPDE data). The pulsed laser was triggered using the electrical pulse generator to ensure the photon arrived during the gate pulse period. SPDE was given by [29]

$$\mathrm{SPDE} = (P_t - P_d) \,/\, \left(1 - \exp\left(-\bar{N}\right)\right),$$

where P_t and P_d are the probability of detecting an event with and without photon injection, respectively. P_t and P_d were obtained experimentally using C_{rate}/f. The DUT's overall photon-counting performance was evaluated using Noise-Equivalent-Power (NEP), defined as

$$\mathrm{NEP} = (h\nu/\mathrm{SPDE})\ \sqrt{2\,\mathrm{DCR}},$$

where $h\nu$ is the photon energy [30].

To obtain the avalanche event's timing, a time-to-amplitude converter (Ortec 566) was used to measure time elapsed between i) the start of the overbias pulse and ii) the triggering time at the discriminator. A synchronization signal controlling the pulsed laser provided the first timing signal and the discriminator (when triggered by avalanche events) provided the second timing signal. Outputs of the time-to-amplitude converter were connected to a multichannel analyzer (Canberra Multiport II), which built up histograms of avalanche event's timing for a given V_{ov}. Each histogram was collected over a fixed duration of 5 minutes. At each V_{ov}, two histograms were collected (in the same measurement session) with the DUT in the dark and under single photon-level illumination. By subtracting the dark histogram from the illuminated histogram, we obtained a histogram associated with photon-initiated avalanche event's timing. The SPDE setup's timing jitter was estimated to be $\sim$116 ps. This was obtained experimentally from the SPDE setup, by measuring

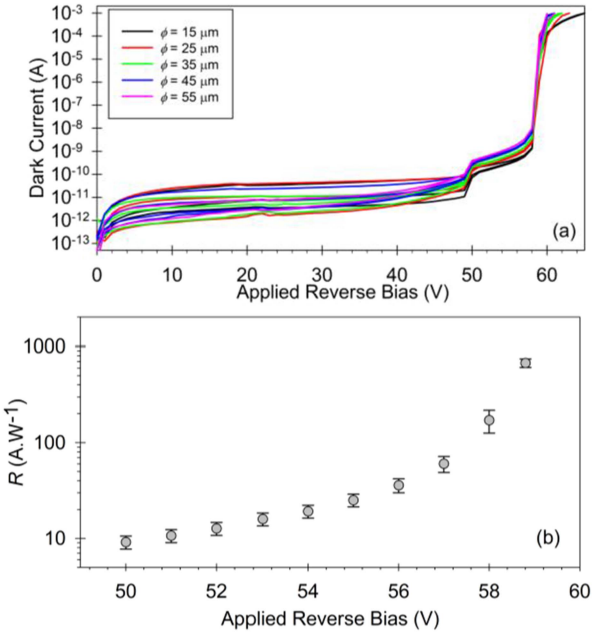

Fig. 1. (a) Reverse dark I-V of 17 devices with diameters of 15 – 55 μm. (b) Mean R(V) from six devices with 55 μm diameter.

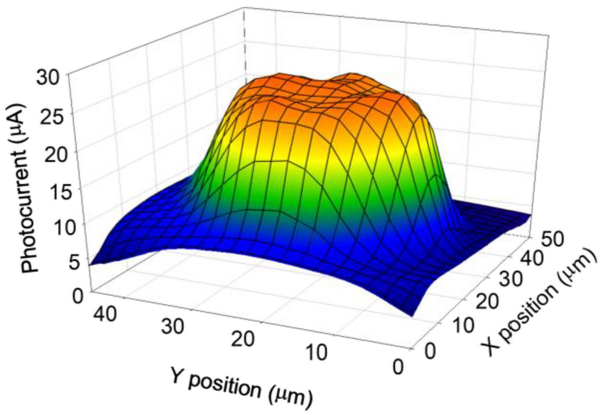

Fig. 2. Raster scan photocurrent of 35 μm diameter device reverse-biased at 58.5 V (0.975 V_{bd}) under 1550 nm illumination.

event's timing distribution from the devices of this work in linear mode and illuminated with the pulsed laser at high optical power (~33 nW average power or 26 $\times 10^6$ photons per pulse). The setup's timing jitter in this work is considerably smaller than our earlier work [25], following the removal of a delay generator with significant timing jitters. Assuming Gaussian distributions for both the setup's and the device's timing jitter, a simple residual sum of squares equation was applied to estimate the device's timing jitter.

III. Results and Discussion

Reverse dark current characteristics from devices (with diameters of 15 to 55 μm) are shown in Fig. 1(a). All the dark currents exhibit a sudden increase at ~50 V (suggesting punchthrough voltage and depletion of InGaAs absorption layer), before an even greater increase at ~60 V (indicating V_{bd}). The dark currents do not scale with the device area, indicating that bulk leakage mechanisms are not the dominant contributing mechanisms at these device sizes. This is not a major surprise since it is plausible that surface leakage current is not completely removed in these mesa-based devices.The ratio of V_{bd} to punchthrough voltage is ~1.2 in this work, similar to those of high-performance InGaAs/InP SPADs (e.g., [12]). The ratio is considerably smaller than the ratio of 2.2 in our earlier work [25], indicating higher doping density in the charge sheet as intended. Hence, the electric field in the InGaAs absorber is likely to be lower in this work compared to the earlier work, which is desirable for suppressing dark carriers and, hence the DCR.

Mean values of R versus voltage from six devices confirm that V_{bd} ~60 V, as shown in Fig. 1(b). The devices exhibit uniform $R(V)$ characteristics and achieve R as high as 676 A/W at 58.87 V. Since the maximum theoretical responsivity at 1550 nm is 1.25A/W, this suggests avalanche gain $\geq$ 540. The avalanche gain at the punchthrough voltage is ~8, much higher than the 1.62 in out earier work [25], confirming higher doping density in the charge sheet of this work. The uniform $R(V)$ data suggest an absence of premature edge breakdown in these devices. To confirm this, data from the photocurrent raster scan of a 35 μm diameter device (biased at $0.975V_{bd}$) are shown in Fig. 2. The highest photocurrents coincide with the device's optical window. The photocurrent signal decreases rapidly as the laser spot moves towards the circular metal contact and then beyond the mesa sidewall. No hot spot was observed on the edge of the mesa. The combined $R(V)$ and raster scan data indicate that the devices exhibit bulk avalanche breakdown and do not suffer from edge breakdowns.

Data of DCR versus overbias obtained from three devices with 35 μm and with 15 μm diameters (in gated mode) are in excellent agreement for a given device diameter, as shown in Fig. 3(a). The data are also consistent with DCR values obtained using free-running mode. For a given overbias, the smaller devices have lower DCR values, which is attributed to smaller bulk dark currents contributing to dark counts. For a given overbias ratio of 3.5%, the DCR values are 19 and 77 M.cs^{-1}, significantly lower than that of ref [25] (~200 Mc.s^{-1}). This is consistent with the expected drop in DCR, as indicated by the larger punchthrough voltage in Fig. 1(a), and smaller device areas used in this work.

Additional gated DCR measurements were carried out on two devices in ambiance without temperature stabilization. The data are presented as P_d versus time in the inset of Fig. 3(a). Other measurement conditions include $V_{ov} = 2.5$ V and 1.5 V (for maximum SPDE) for the 15 μm and 35 μm devices, respectively, $f = 10$ kHz and $t_{on} = 20$ ns (same as the main DCR measurements). Values of P_d remained stable over each continuous 2-hour session, at 0.20 (15 μm device) and 0.24 (35 μm device) with standard deviations of ± 1%. These confirm that the operating overbias of AlGaAsSb SPADs are highly stable without any temperature stabilization.

SPDE versus overbias data for the same six devices are compared in Fig. 3(b). At high overbias, extraction of SPDE values

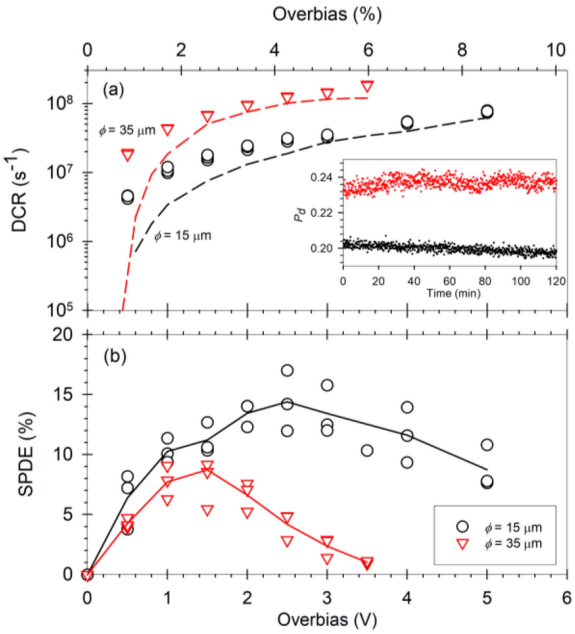

Fig. 3. (a) DCR data versus overbias from 6 devices operated in gated mode (symbols) and in free-running mode (lines). (Inset) P_d versus time data of Ø = 15 and 30 μm devices at $V_{ov} = 2.5$ V without thermal stabilization. (b) SPDE data (symbols) and mean values (lines) versus overbias from the same 6 devices.

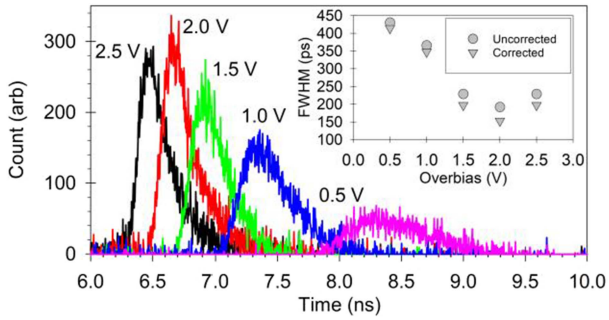

Fig. 4. Histograms of photon-initated avalanche events timings for a 15 μm diamter device with $V_{ov} = 0.5$ V – 2.5 V. (inset) Measured and corrected FWHM of the device versus V_{ov}.

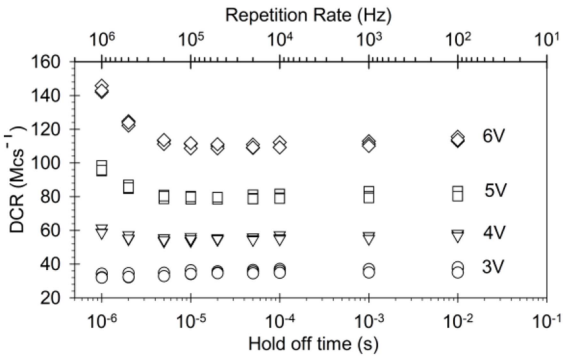

Fig. 5. Dark Count Rate versus repetition rate characteristics for three 15 μm diameter devices at 300 K.

(which relies on subtraction of dark counts from counts with illumination) was affected by high DCR values. A maximum of one count would be recorded for each overbias pulse, so increased dark counts at high overbias prevented some photon counts to be registered. Hence SPDE values tend to increase with the overbias, reaching a maximum value (the exact value vary with device diameter and t_{on}) before decreasing with overbias. Again, SPDE values are in agreement with a given device diameter. Using mean SPDE values, the maxima are ~9 and 14% at $V_{ov} = 1.5$ and 2.5 V, for the 35 and 15 μm diameter devices, respectively. The corresponding DCR values (and P_d) are 68 and 30 Mc.s^{-1} (0.64 and 0.41), respectively. These SPDE data represent a significant improvement over the previous (and first) report of InGaAs/AlGaAsSb APD for single photon detection, which was unable to detect single photon at room temperature due to much higher DCR [25].

The timing performance of the devices is evaluated using histograms of photon-initiated avalanche event's timing obtained from a 15 μm diameter device at varying V_{ov}, as shown in Fig. 4. As V_{ov} increases, the total count for each histogram increases because of increasing avalanche event probability, as observed in the increasing SPDE. Full-Width-Half-Maximum (FWHM) values of the histograms for $V_{ov} = 0.5$ to 2.5 V reduce from 430 to 230 ps. The minimum FWHM measured was 190 ps and occurred at $V_{ov} = 2$ V. Taking into account the setup's timing jitter, the corrected timing jitter of the devices for $V_{ov} =$ 0.5 to 2.5 V is 410 to 150 ps, as shown in inset of Fig. 4. The device's timing jitter worsens when V_{ov} increases from 2.0 to 2.5 V, probably due to data uncreatinity caused by increase in the dark histogram at higher V_{ov}.The timing jitter values of this work match those of commercial InGaAs/InP SPADs (e.g., 130 ps at 32% SPDE [31]). It is noted that the timing jitter values in this work were obtained using $\bar{N} = 0.1$, yet are already better than those of recent Ge/Si SPADs which were obtained using non-single photon conditions ($\bar{N} = 10$ and 207 ps [22]; $\bar{N} =$ 955 and 159 ps [23]).

Afterpulsing data from three 15 μm devices are presented as DCR versus hold-off time (lower) or gate repetition rate (upper axis) as a function of overbias in Fig. 5. The DCR values are highly uniform from device to device. At $V_{ov} = 3$ V, they are constant for hold-off times as short as 1 μs (repetition rate as high as 1 MHz). The extent of afterpulsing is much reduced compared to our earlier work [25] (requiring hold-off time > 5 μs at $V_{ov} = 3$ V and 200 K), owing to the considerably higher operation temperature in this work.

NEP values are useful performance indicators for SPADs because they consider both DCR and SPDE. The mean NEP (with standard deviation shown in error bars) versus overbias of this work is presented in Fig. 6(a). NEP of the 15 μm diameter devices does not vary significantly between $V_{ov} = 0.5$ to 2.5 V and are comparable to the 200 K NEP value from earlier InGaAs/AlGaAsSb SPAD [25]. It is worth noting that in this work no afterpulsing effects was observed up to $V_{ov} = 3$ V and the smallest timing jitter was observed at $V_{ov} = 2.0$ V. Hence the optimum V_{ov} is ~2 V for the 15 μm diameter devices.

The NEP values of this work are compared with other room temperature SPADs made with InGaAs/InP, InGaAs/InAlAs and Ge/Si in Fig. 6(b). InGaAs/AlGaAsSb SPADs of this work have

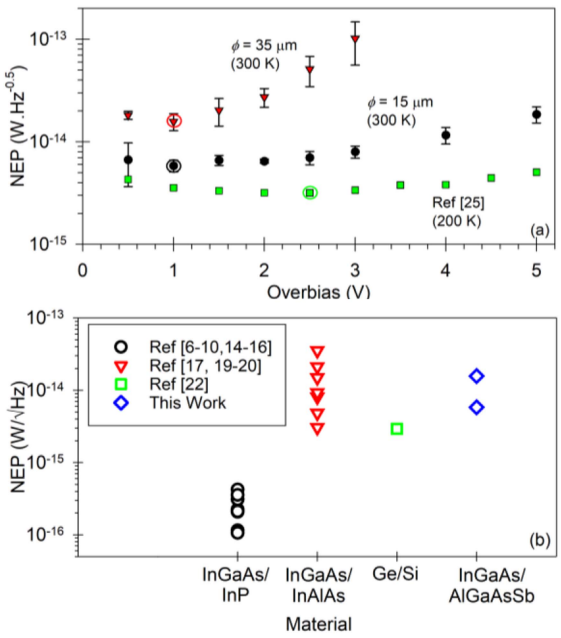

Fig. 6. (a) NEP versus overbias data for this work (300 K) and previous InGaAs/AlGaAsSb SPADs (200 K) [25]. (b) Room temperature best NEP values of SPADs made with InGaAs/InP, InGaAs/InAlAs, Ge/Si, and InGaAs/AlGaAsSb. All data were for 1550 nm wavelength, except for the Ge/Si SPAD (1310 nm).

higher NEP values than those of InGaAs/InP SPADs by an order of magnitude but are comparable to InGaAs/InAlAs SPAD. The values of this work are similar to that of Ge/Si SPAD measured at 1310 nm wavelength [22]. Ge/Si SPAD from ref [23] is excluded from Fig. 6(b) because their measurements did not use single photon conditions.

SPDE values of Ge/Si SPADs are expected to reduce as the wavelength increases from 1310 to 1550 nm, worsening their NEP values due to reduced photon absorption efficiency. Hence, the difference in NEP values between Ge/Si SPADs and InGaAs/AlGaAsSb SPADs is likely to reduce when compared at 1550 nm wavelength. To improve performance of future InGaAs/AlGaAsSb SPADs, incorporating optical cavity and anti-reflection coating to increase SPDE values should be considered. Considering that the best NEP values and peak SPDE values occur at small overbias values, addressing DCR would be worthwhile, so further efforts should also investigate the dominant cause(s) of DCR and/or refining electric profiles in InGaAs/AlGaAsSb SPADs.

IV. Conclusion

Room temperature single photon detection characterization at 1550 nm wavelength was carried out on multiple InGaAs/AlGaAsSb SPADs operated in gated mode. In linear mode, the devices achieved avalanche gain ≥ 540 prior to breakdown and did not show signs of edge breakdowns. In Geiger mode and using 0.1 photons per pulse, the maximum SPDE was 14 and 9% with DCR of 30 and 68 Mc.s^{-1}, for 15 and 35 μm diameter devices, respectively. The resultant NEP values are around an order of magnitude higher than those of InGaAs/InP SPADs, but are comparable to InGaAs/InAlAs SPAD. For overbias up to 3 V and repetition rate up to 1 MHz, the DCR was unaffected by afterpulsing. Timing jitters were as low as 150 ps (at $V_{ov} = 2.0$ V), matching the performance of InGaAs/InP SPADs and exceeding those of Ge/Si SPADs. These results represent a significant improvement over the earlier InGaAs/AlGaAsSb SPADs, which was unable to detect single photon at room temperature. With further optimization in device features and research into dominant DCR mechanism(s), InGaAs/AlGaAsSb SPADs could be a suitable candidate as practical single photon detectors for room temperature operation.

References

[1] N. Gisin, G. Ribordy, W. Tittel, and H. Zbinden, "Quantum cryptography," *Rev. Modern Phys.*, vol. 74, no. 1, pp. 145–195, 2002, doi: 10.1103/RevModPhys.74.145.

[2] S. K. Poultney, "Single photon detection and timing in the lunar laser ranging experiment," *IEEE Trans. Nucl. Sci.*, vol. TNS-19, no. 3, pp. 12–17, Jun. 1972, doi: 10.1109/TNS.1972.4326697.

[3] Q. Zhou, Z. Tan, and C. Yang, "Theoretical limit evaluation of ranging accuracy and power for LiDAR systems in autonomous cars," *Proc. SPIE*, vol. 57, no. 9, Sep. 2018, Art. no. 096104, doi: 10.1117/1.OE.57.9.096104.

[4] J. Titchener et al., "Single photon lidar gas imagers for practical and widespread continuous methane monitoring," *Appl. Energy*, vol. 306, Jan. 2022, Art. no. 118086, doi: 10.1016/j.apenergy.2021.118086.

[5] K. M. Rosfjord et al., "Nanowire single-photon detector with an integrated optical cavity and anti-reflection coating," *Opt. Exp.*, vol. 14, no. 2, pp. 527–534, 2006, doi: 10.1364/OPEX.14.000527.

[6] Y.-Q. Fang et al., "InGaAs/InP single-photon detectors with 60% detection efficiency at 1550 nm," *Rev. Sci. Instrum.*, vol. 91, no. 8, Aug. 2020, Art. no. 083102, doi: 10.1063/5.0014123.

[7] S.-H. Baek, S.-C. Yang, C.-Y. Park, C.-W. Park, S.-B. Cho, and S.-W. Ryu, "Room temperature quantum key distribution characteristics of low-noise InGaAs/InP single-photon avalanche diode," *J. Korean Phys. Soc.*, vol. 78, no. 7, pp. 634–641, Apr. 2021, doi: 10.1007/s40042-021-00111-4.

[8] H. Chen, M. Jiang, S. Sun, G. Tang, and L. Liang, "Room temperature continuous frequency tuning InGaAs/InP single-photon detector," *Amer. Inst. Phys. Adv.*, vol. 8, no. 7, Jul. 2018, Art. no. 075106, doi: 10.1063/1.5030141.

[9] J. Li et al., "Design of a room-temperature, sine-wave gated, InGaAs/InP SPAD based photon counting system with dead-time mitigation," *J. Light. Technol.*, vol. 42, no. 8, pp. 2887–2893, Apr. 2024, doi: 10.1109/JLT.2023.3332480.

[10] E. Kizilkan et al., "Guard-ring-free InGaAs/InP single-photon avalanche diode based on a novel one-step Zn-diffusion technique," *IEEE J. Sel. Topics Quantum Electron.*, vol. 28, no. 5, Sep./Oct. 2022, Art. no. 9300209, doi: 10.1109/JSTQE.2022.3162527.

[11] S. Pellegrini et al., "Design and performance of an InGaAs–InP single-photon avalanche diode detector," *IEEE J. Quantum Electron.*, vol. 42, no. 4, pp. 397–403, Apr. 2006, doi: 10.1109/JQE.2006.871067.

[12] F. Signorelli et al., "Low-noise InGaAs/InP single-photon avalanche diodes for Fiber-based and free-space applications," *IEEE J. Sel. Topics Quantum Electron.*, vol. 28, no. 2, Mar./Apr. 2022, Art. no. 3801310, doi: 10.1109/JSTQE.2021.3104962.

[13] T. He, X. Yang, Y. Tang, R. Wang, and Y. Liu, "High photon detection efficiency InGaAs/InP single photon avalanche diode at 250 K," *J. Semicond.*, vol. 43, no. 10, Oct. 2022, Art. no. 102301, doi: 10.1088/1674-4926/43/10/102301.

[14] A. Tada, N. Namekata, and S. Inoue, "Saturated detection efficiency of single-photon detector based on an InGaAs/InP single-photon avalanche diode gated with a large-amplitude sinusoidal voltage," *Jpn. J. Appl. Phys.*, vol. 59, no. 7, Jul. 2020, Art. no. 072004, doi: 10.35848/1347-4065/ab9625.

[15] L. C. Comandar et al., "Gigahertz-gated InGaAs/InP single-photon detector with detection efficiency exceeding 55% at 1550 nm," *J. Appl. Phys.*, vol. 117, no. 8, Feb. 2015, Art. no. 083109, doi: 10.1063/1.4913527.

[16] Y. Liang, Y. Jian, X. Chen, G. Wu, E. Wu, and H. Zeng, "Room-temperature single-photon detector based on InGaAs/InP avalanche photodiode with multichannel counting ability," *IEEE Photon. Technol. Lett.*, vol. 23, no. 2, pp. 115–117, Jan. 2011, doi: 10.1109/LPT.2010.2092756.

[17] Y. Tian et al., "High speed and high sensitivity InGaAs/InAlAs single photon avalanche diodes for photon counting communication," *J. Light. Technol.*, vol. 40, no. 15, pp. 5245–5253, Aug. 2022, doi: 10.1109/JLT.2022.3174962.

[18] X. Meng et al., "InGaAs/InAlAs single photon avalanche diode for 1550 nm photons," *Roy. Soc. Open Sci.*, vol. 3, no. 3, Mar. 2016, Art. no. 150584, doi: 10.1098/rsos.150584.

[19] X. Meng, C. H. Tan, S. Dimler, J. P. R. David, and J. S. Ng, "1550 nm InGaAs/InAlAs single photon avalanche diode at room temperature," *Opt. Exp.*, vol. 22, no. 19, Sep. 2014, Art. no. 22608, doi: 10.1364/OE.22.022608.

[20] Y.-S. Lee et al., "$In_{0.52}Al_{0.48}As$ based single photon avalanche diodes with stepped E-field in multiplication layers and high efficiency beyond 60%," *IEEE J. Sel. Topics Quantum Electron.*, vol. 28, no. 2, Mar./Apr. 2022, Art. no. 3802107, doi: 10.1109/JSTQE.2021.3114130.

[21] Y.-S. Lee, P.-L. Wu, Y.-J. Chen, and J.-W. Shi, "Neat temporal performance of InGaAs/InAlAs single photon avalanche diode with stepwise electric field in multiplication layers," *IEEE Access*, vol. 9, pp. 32979–32985, 2021, doi: 10.1109/ACCESS.2021.3060824.

[22] N. Na et al., "Room temperature operation of germanium–silicon single-photon avalanche diode," *Nature*, vol. 627, no. 8003, pp. 295–300, Mar. 2024, doi: 10.1038/s41586-024-07076-x.

[23] C.-E. Chen et al., "High temperature tolerant Ge-on-Si single photon avalanche diode at the communication wavelength," *IEEE Electron Device Lett.*, vol. 45, no. 8, pp. 1413–1416, Aug. 2024, doi: 10.1109/LED.2024.3416186.

[24] Phlux Technology Ltd (2023), "phlux-aura-datasheet-30um," 2023. Accessed: Apr. 12, 2024. [Online]. Available: https://phluxtechnology.com/assets/general/phlux-aura-datasheet-30um_2024-01-24-130406_zymd.pdf

[25] J. Taylor-Mew, X. Collins, B. White, C. H. Tan, and J. S. Ng, "Development of InGaAs/AlGaAsSb Geiger mode avalanche photodiodes," *IEEE Trans. Electron Devices*, vol. 71, no. 3, pp. 1994–1998, Mar. 2024, doi: 10.1109/TED.2024.3354698.

[26] Y. Cao, T. Osman, E. Clarke, P. K. Patil, J. S. Ng, and C. H. Tan, "A GaAsSb/AlGaAsSb avalanche photodiode with a very small temperature coefficient of breakdown voltage," *J. Light. Technol.*, vol. 40, no. 14, pp. 4709–4713, Jul. 2022, doi: 10.1109/JLT.2022.3167268.

[27] J. D. Taylor-Mew, L. Li, C. H. Tan, and J. S. Ng, "Room temperature InGaAs/AlGaAsSb single photon avalanche diode: Dataset and figures," The University of Sheffield, doi: 10.15131/shef.data.27325509.

[28] S. J. Dimler, J. S. Ng, R. C. Tozer, G. J. Rees, and J. P. R. David, "Capacitive quenching measurement circuit for Geiger-mode avalanche photodiodes," *IEEE J. Sel. Topics Quantum Electron.*, vol. 13, no. 4, pp. 919–925, Jul./Aug. 2007, doi: 10.1109/JSTQE.2007.903595.

[29] Y. Kang, H. X. Lu, Y.-H. Lo, D. S. Bethune, and W. P. Risk, "Dark count probability and quantum efficiency of avalanche photodiodes for single-photon detection," *Appl. Phys. Lett.*, vol. 83, no. 14, pp. 2955–2957, Oct. 2003, doi: 10.1063/1.1616666.

[30] M. Ghioni, A. Gulinatti, I. Rech, P. Maccagnani, and S. Cova, "Large-area low-jitter silicon single photon avalanche diodes," *Proc. SPIE*, vol. 6900, Feb. 2008, Art. no. 69001D, doi: 10.1117/12.761578.

[31] Micro Photon Devices "PDM-IR," 2022. Accessed: Oct. 24, 2022. [Online]. Available: http://www.micro-photon-devices.com/Products/Photon-Counters/PDM-IR